

Hydrogen Oxidation-Mediated Current Discharge in Mesoporous Pt/TiO₂ Nanocomposite

*Nathan J. Ray and Eduard G. Karpov**

Department of Civil and Materials Engineering, University of Illinois at Chicago, Chicago, Illinois, 60607, USA

KEYWORDS Mesoporous titania, plasma electrolytic oxidation, reaction current, proton spillover

Here we report on direct evidence of a correlation between hydrogen-to-water oxidation on mesoporous Pt/TiO₂ nanocomposites at room temperature and the conversion of surface released chemical energy into a stationary electrical current. The Pt phase of this heterojunction device is an electrically continuous 15-nm thick mesh deposited onto a mesoporous TiO₂ substrate fabricated with a plasma electrolytic oxidation process. The H₂O turnover frequency approaches an asymptotic value associated with the saturation of the Pt/TiO₂ interface as the concentration of hydrogen gas is increased. *In situ* measurements of the reaction-induced current concurrently with mass spectrometry measurements illuminate the polarity switch of the reaction current (from thermionic emission to a reverse steady-state flow) simultaneously with the production of water. Furthermore, a concentration-dependent value of 5 minutes is measured as the time constant for the adsorption of the initial addition of H₂ and H₂O formation and desorption.

1. Introduction

As growing importance is being placed on areas such as fuel cells¹⁻⁵, solid-state chemical sensors⁶⁻¹¹, photocatalysis¹²⁻¹³, and many other solid-state power generators, it is becoming increasingly important to investigate and understand surface-driven catalytic processes of bifunctional systems. Within these processes, excited-state transport induced by the oxidation of hydrogen to water on the surface of metal/metal oxide heterojunction nanocomposites offers many enticing possibilities for power generation applications. These metal/metal oxide heterojunctions exhibit beneficial electrical and interfacial properties when we consider the junction of a catalytic metal and a semiconductor. Deposition of nanodispersed catalytic metals on various semiconducting substrates is advantageous due to inherent electrical and optical properties of such nanodispersed metals, in addition to the obvious advantage of a higher surface area to volume ratio for surface driven catalysis applications.

Chemical reaction-induced currents have long been an area of interest, with much research devoted to the determination of the underlying mechanisms of these currents. Hagemann et al. have contributed many such studies on the Mg/Si system. During the deposition of Mg onto Mg/*p*-Si(001), chemically-induced current (referred to as chemicurrent) was measured and found to be exponentially attenuated with increasing Mg film thickness.¹⁴ The attenuation length was found to be 5 nm, a typical value for hot electron transport in metal films. Upon further investigation of this system, the reactivity of the Mg film with molecular oxygen was characterized.¹⁵ This reactivity was found to be a function of the Mg film thickness, with chemicurrent resulting from Mg oxidation exhibiting a maximum for Mg film thickness of 9 and 13 monolayers.

Among systems consisting of catalytic metal deposition on semiconducting substrates, recently much focus has been placed on the active chemical transducer Pt/TiO₂.¹⁶⁻²⁸ This system shows

great potential through its ability to convert excessive surface-released chemical energy into an electric current in an electrolyte-free system. In these Pt/TiO₂/Ti electromotive force (emf) cells, hot electron flow over the Schottky barrier (ballistic transport) has been investigated under various oxyhydrogen environments.¹⁷⁻²⁶ Recently, Lee et al.²⁴ investigated hot electron transfer within nanodiode composites due to hydrogen oxidation occurring on platinum nanoparticles. The nanodiodes of interest consisted of a single layer of graphene grown on top of TiO₂ with a two-dimensional array of Pt nanoparticles deposited on the graphene layer. Using this geometry, it was shown that the flow of hot electrons when these structures were subjected to oxyhydrogen environments mirrored the kinetics of the catalytic reaction.

More recently, a deeper understanding of the thermal properties of these nanocomposite systems has been sought, with research into what role H₂O plays when these Pt/TiO₂/Ti emf cells are in use. In a work by Cakabay et al.²⁵, microcalorimetry was utilized to investigate the temperature dependence of surface reaction-generated current during the oxidation of hydrogen. They report on the generation of elevated and constant current magnitudes for temperatures within a kinetic region associated with mass transport and catalytic activity. Cakabay et al.²⁶ then studied the reaction current generation of Pt/TiO₂/Ti systems under an oxyhydrogen environment as the relative humidity level was varied. They found that the short-circuit current of this cell displayed a maximum value for a relative humidity of 10%, and that current decreased with further increasing humidity. Furthermore, the open-circuit voltage strictly increased as the relative humidity increased.

We report on the water production of a Pt/TiO₂/Ti nanocomposite system and we investigate the underlying mechanism dictating *room-temperature* stationary current observed with this

electrolyte-free chemical transducer. We further show that the water turnover frequency approaches a constant limiting value as the gaseous-phase hydrogen is increased.

2. Experimental Methods

Mesoporous TiO₂ films were grown anodically via plasma electrolytic oxidation (PEO), with synthesis techniques reported elsewhere.^{17, 21–22} An aqueous electrolyte of 3M H₂SO₄ was used in the galvanostatic PEO (current density = 93.2 mA/cm²) of 36 x 12 x 0.5 mm³ strips of 0.989 pure titanium metal, with the Ti strips acting as the anode fastened parallel to a 153 x 26 x 6 mm³ graphite cathode. After the first three minutes of the process had elapsed, the potential difference had increased to ~95 V, upon which time micro-arc discharges became visible on the surface of the Ti anode. These arcs result in a volumetric region of highly intense electric field with elevated temperature, and consequently lead to a self-assembled mesoporous morphology. Locally the process is volatile and erratic; however the result is homogeneous and uniform on a larger scale. The voltage reached a stable value of 150 V after 15 min, and in the ensuing 5 min the voltage approached 155 ± 2 V. The Ti substrates were allowed to anodize for 20 min, after which the process was halted abruptly, resulting in a mesoporous TiO₂ layer of 10 – 11 μm thickness. Systematic studies of the oxide thickness using a destructive technique were performed for previous publications.^{17, 21} In the present work, the same oxidation procedure and parameters were used to produce oxide films of equivalent thickness. Schierbaum et al.²⁰ examined microscopic images of sample cross sections that had been anodized at different voltages, using a similar PEO technique, and found the titania layer thickness varied between 1.8 μm and 7.0 μm as the potential difference of the electrochemical cell varied between 60 V and 170 V. These measurements are in agreement with our own, with the slight difference in oxide thickness attributed to the difference in electrolyte concentration used.

The metal-semiconductor heterojunction was then fabricated by depositing an electrically continuous mesh-like Pt nanogranular structure onto the TiO₂ surface via wide-angle physical vapor deposition (PVD) sputtering at a constant rate of 0.02 nm·s⁻¹. The Pt film thickness was measured by an Inficon quartz microbalance, and the deposition was aborted by closing the source shutter when the Pt mesh reached an equivalent thickness of 15 nm, as would be the case during deposition onto a planar surface. We refer the reader to references [17, 21] for further sample fabrication and characterization details.

SEM micrographs taken of the TiO₂ surface without Pt deposition in (A), and with Pt deposition in (B), are shown in Figure 1. The Pt layer displays the same surface morphology as the underlying TiO₂, thus providing topographical mesh. Resistance measurements confirm in-plane electrical continuity across the Pt film. To characterize the porous Pt/TiO₂ composite, focused ion beam milling was performed. Figures 1 (C) – (D) present the milling at two different penetration depths to provide a depth profile for the pores. It is seen that even at an average depth of 1.5 μm, pores remain and penetrate further into the sample. SEM-grade silver paste was then used to fasten two 0.25 mm diameter silver wires to the ends of the Pt mesh, resulting in 2.8 cm² of exposed Pt that served as the effective active area to support catalytic surface reactions.

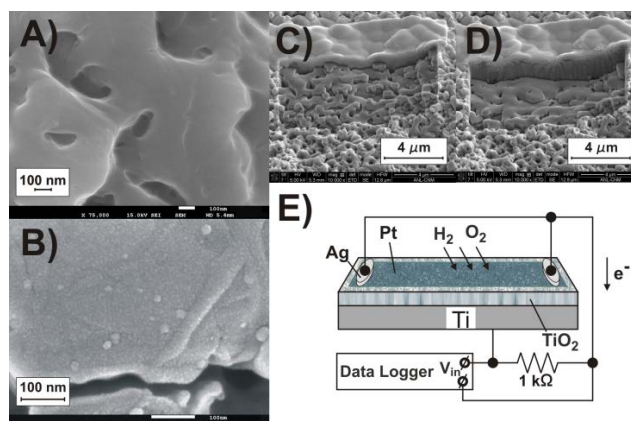


Figure 1. SEM micrographs of TiO₂ synthesized via PEO, both before Pt deposition (A) and after deposition of Pt (B). Ion milling in (C) – (D) reveals porosity depth profile. (E) depicts sample geometry with reaction current measurement circuit; the data logger (+) V terminal is on the Pt phase.

A resistive temperature sensor (Omega F2020–100) was positioned on the middle of the Pt film under the support of its connection wires only to avoid any adhesive contaminants, after which the fabricated samples were placed in a 4.5 liter analytical chamber with residual pressure $< 10^{-6}$ Torr. A depiction of the sample structure with the external circuit is given in Figure 1 (E). The current generated by surface reactions on the sample was routed through a 1 k Ω resistor connected in parallel with a data logging device. The electrical terminals during data acquisition were the Pt phase and the Ti substrate, with the (+) V terminal on the Pt mesh.

Prior to data collection all samples were activated through a heat treatment. The samples were maintained under an environment consisting of 160 Torr oxygen and 16 Torr hydrogen, and subsequent thermal activation was initiated through the use of two parallel-connected halogen bulbs (12 V/100 W) positioned at a distance 5 mm from the Pt surface. The surface temperature of the sample was increased to 50 °C at a rate of 4 – 5 °C·min⁻¹, after which reaction current was detected. The heat treatment was terminated at this point and the initiated reaction was allowed to proceed undisturbed, resulting in a surface temperature increase to 180 – 210 °C. Following this

one-time activation procedure, all further reactions in oxyhydrogen environments with a given sample were carried out at *room temperature*.

3. Results and Discussion

The samples were analyzed in batch reactor mode, with gas admittance executed diffusively at a rate of $2 - 3 \text{ Torr}\cdot\text{s}^{-1}$. 160 Torr O_2 was firstly admitted to the chamber with an initial pressure $< 10^{-6}$ Torr, and following a waiting period of 1 - 2 min 16 Torr H_2 was added to the system. Upon this first hydrogen admission, several autonomous features in the chemically-driven current arise in a regime we refer to as the *fast reaction*; these features have been well documented previously.¹⁷ At the onset of this fast reaction, the negative current generated reflects an interaction of the adsorbed oxygen and the gas-phase hydrogen. This exothermic reaction causes rapid Pt surface temperature increase to $180 - 210 \text{ }^\circ\text{C}$, thus generating a positive-biased current due to hot electron generation and thermionic emission. As hydrogen molecules adsorb onto the surface, disassociation occurs and the hydrogen atoms may ionize due to high electronegativity of the Pt phase. The released electrons flow through the external circuit and arrive at the TiO_2 conduction band. The total pressure, temperature, and reaction current kinetics throughout this process are given in Figure 2; the time-axis scale is the same in all three panels.

As the sample surface returns to room temperature 15 – 20 min after the fast reaction began, it provokes a robust and long-standing *stationary* electrical signal in what we refer to as the slow reaction mode. This mode remains in place beyond time $t \approx 17$ min, as can be seen in the bottom panel of Figure 2. While in this mode, negative charge is transferred from the *n*-type TiO_2 toward the Pt phase. It has been proposed^{17, 21–22} that the source of this stationary current is the

proton spillover mechanism. As H^+ ions diffuse to the Pt/TiO₂/gas interface through an *excited-state transport* mechanism, they may spill over onto the TiO₂ phase according to



Protons that are consequently chemisorbed on the TiO₂ surface can then recombine with conduction band electrons, producing the standard cathodic reaction



At times 100, 130, 160, 190, and 220 min after the primary addition of hydrogen, additional 4 Torr H₂ was added to the system. The electronic conductance of the *n*-type TiO₂ increases with decreasing oxygen partial pressure relative to the total pressure, and as a result a step-like increase of the stationary current is observed with these additions of H₂ as seen in the bottom panel of Figure 2. The slight temperature increase with each 4 Torr H₂ addition, shown in the Figure 2 inset, coincides with the increase of the reaction current output. The resistance of freshly deposited Pt film is approximately 560 Ω, and that value decreases abruptly to a stable value of about 340 Ω after the first reaction, suggesting a one-time recrystallization process. The in-plane resistance change is nearly negligible thereafter, changing less than 1 – 2 Ω after weeks of repeated experiments – thus illustrating the long-term stability of this system. For this work, we place the focus of our investigation on the water production as a result of the catalytic reaction occurring on the sample surface.

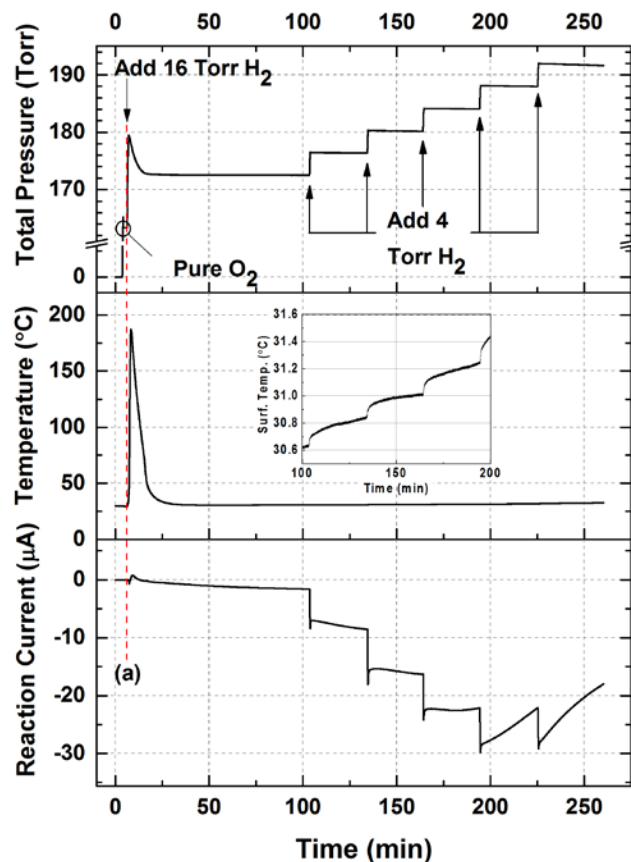


Figure 2. Total pressure, temperature, and reaction current kinetics from Pt/TiO₂/Ti sample after 6 additions of H₂ to an initially pure O₂ environment. All plots have same time scale, and inset gives finer resolution to the temperature increase during three additions of 4 Torr H₂. The vertical dashed line (a) indicates the addition of 16 Torr H₂.

Additions of 4 Torr H₂ (as seen in the top panel of Figure 2) will be henceforth referred to in sequential order as Step 1, Step 2, etc., and are labeled as such in the following figures; Step 0 defines the slow reaction regime as the current approaches a steady-state value. These step-wise additions of hydrogen occurred on thirty minute intervals, with mass spectrometry utilized to measure the H₂O kinetics in the exhaust gas mixture throughout the entire process, as displayed in Figure 3. The exhaust mixture pressure in the mass spectrometry chamber was maintained at 3×10^{-5} Torr, rendering the total pressure drop over any one step negligible (the total pressure drop over a 30 min step was less than 0.1 Torr, while the total pressure was 172 Torr at the end of Step 0 and

increased thereafter with further 4 Torr H₂ additions). During the fast reaction, hydrogen “burn-out” occurs as the catalytic Pt surface initiates hydrogen oxidation. As seen in Figure 3 (B) this leads to a characteristic increase in water vapor initially, with a rate decrease occurring about 25 min later.

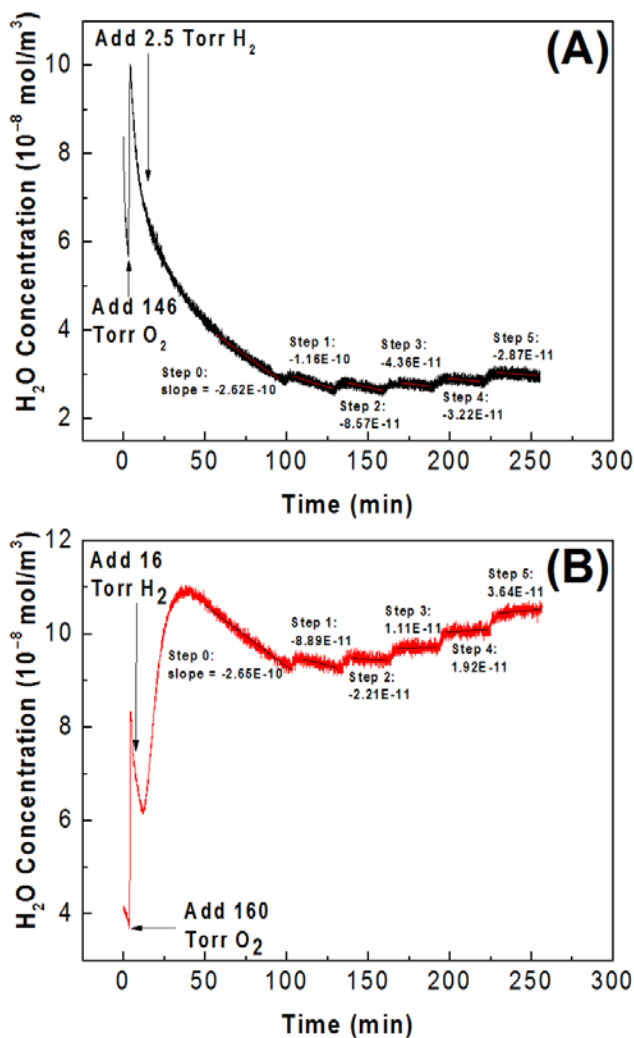


Figure 3. H₂O kinetics as measured by mass spectrometry. The concentration in (A) was measured with *no sample* present in the chamber, while H₂O kinetics with Pt/TiO₂/Ti sample is displayed in (B). In both (A) and (B) the linear regressions are shown with the accompanying slopes.

The measurement of interest was the water turnover frequency (TOF) of this nanocomposite system during the generation of the stationary current. For the oxidation of hydrogen depicted in Eqn. (3), the rate of water production can be described as

$$r_{\text{H}_2\text{O}} = \frac{d}{dt} [\text{C}_{\text{H}_2\text{O}}] , \quad (4)$$

where $\text{C}_{\text{H}_2\text{O}}$ is the water vapor concentration. This rate is readily available from the mass spectrometry data through differentiation of the linear best fit lines which are shown in Figure 3. However, we should not assume the analysis chamber is inert, and consequently the water concentration measurement with a sample in the analysis chamber represents the water production of the sample itself plus water production that occurred on the chamber walls,

$$r_{\text{meas}} = r_{\text{ambient}} + r_{\text{Pt/TiO}_2}, \quad (5)$$

where r_{meas} is the measurable water production rate, r_{ambient} is the ambient component due to the chamber walls, and $r_{\text{Pt/TiO}_2}$ is the water produced by the sample. To account for this, the ambient water production rates must be subtracted from those which were measured with Pt/TiO₂ samples present.

To replicate the oxyhydrogen environment after hydrogen burn-out had occurred on the sample, in the experiment without a sample present in the chamber the O₂ and H₂ partial pressures were matched to those of the sample after the fast reaction had occurred, but prior to Step 1 at $t \approx 100$ min, thus necessitating the addition of 146 Torr O₂ and 2.5 Torr H₂. Additionally, the water rate of change was also matched prior to Step 1 for both cases, again referring back to the concentration gradients of Step 0 shown in Figure 3. Worth mentioning was that due to the nature

of the catalytic surface reaction, the water partial pressure was not equivalent for the two experiments.

Utilizing Eqn. (5) to solve for $r_{\text{Pt/TiO}_2}$, the ambient water production rates seen in Figure 3 (A) were subtracted from the rates measured with a sample present, Figure 3 (B). The water TOF resulting from this difference $r_{\text{meas}} - r_{\text{ambient}}$ thus yields the water TOF due to the Pt/TiO₂/Ti nanocomposite and is given in Figure 4, where the error bars are attributed to higher adsorption rates on the chamber walls due to the increased humidity levels. It is observed that at lower H₂ concentrations, additional H₂ increases the water TOF. However, the TOF starts to asymptotically approach a constant value for higher H₂ concentrations, which is ascribed to the saturation of the Pt/TiO₂/reactive gas interface. The TOF decrease in Steps 3 and 4 is within the range of the error bars, thus supporting the assertion that water turnover frequency is indeed approaching a limiting asymptote. In agreement with the findings by Cakabay et al.²⁶, we make the observation that as the H₂O TOF approaches this asymptotic value between Step 2 and Step 3, the chemically-induced current also experiences an inflection point during Step 3 and begins to decrease thereafter, as seen in the bottom panel of Figure 2. This may be the effect of wetting, or to a small extent water poisoning, as the Pt/TiO₂ interface becomes increasingly saturated with water, in which case water desorption may play a crucial role in the reaction current magnitude.

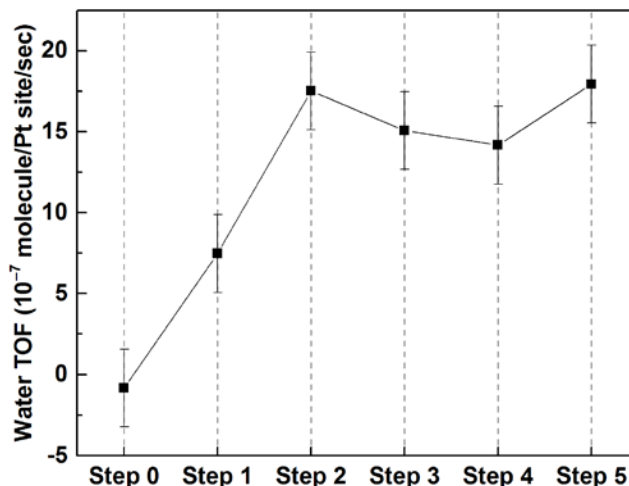


Figure 4. H₂O turnover frequency as function of 4 Torr hydrogen steps.

Prior to analysis of the Pt/TiO₂/Ti system, however, we first demonstrated the absence of any potential contribution to water production from the Ag contacts and due to the gas/TiO₂ interface. For this purpose, a sample was synthesized with geometry identical to Figure 1 (E), except the 15 nm Pt film was not deposited on the TiO₂ surface. Thus the resultant geometry was a TiO₂/Ti structure with two silver contacts applied directly to the TiO₂ surface. This sample was then placed into the analysis chamber and subjected to the same oxyhydrogen conditions outlined previously. Mass spectrometry of the exhaust gas mixture was performed to measure the H₂O kinetics. As shown in Figure 5, the addition of 160 Torr O₂ induces a spike in water concentration which then asymptotically decays in spite of the introduction of 16 Torr H₂. The linear regressions and accompanying slopes are also depicted in Figure 5. Further additions of 4 Torr hydrogen at times 100, 130, 160, 190, and 220 min marginally increase the rate of water production, but it is seen that the water concentration rate remains negative throughout the process. Noting that the water concentration in the case of a sample without the Pt film, Figure 5, and the case without a sample present in the chamber, Figure 3(A), are nearly identical, we conclude that the Ag contacts are not catalytic and do not contribute appreciably to water formation. Therefore, having accounted

for water production due to the analysis chamber walls as well as contributions attributed to the Ag phase present, we conclude that the water TOF shown in Figure 4 is the true H₂O TOF induced by the Pt/TiO₂/Ti nanocomposite.

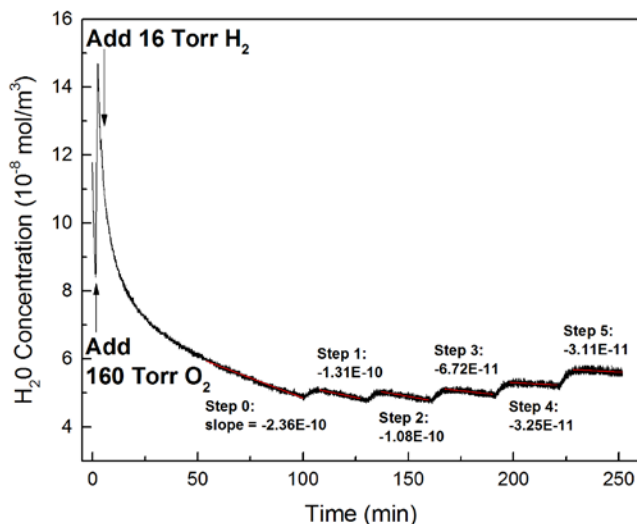


Figure 5. H₂O kinetics as measured by mass spectrometry with a sample lacking the Pt film. The linear regressions are shown with the accompanying slopes.

Of interest are the time delays presented by the data during the fast reaction regime, as can be seen in Figure 6. Note that the partial exhaust H₂O pressure is the same data shown in Figure 3 (B), albeit in different units, and as such the local minima for water observed at $t \approx 12$ min in Figure 6 is the same local minima seen in Figure 3 (B). All time differences were calculated from the inflection points of the curves. Upon the initial 160 Torr O₂ addition, the data shows an immediate increase in both the chamber total pressure and the partial pressure in the exhaust gas. H₂ followed a similar trend, although there was a 40 second delay between the detection of hydrogen by the capacitive pressure transducers in the chamber and a response in the mass

spectrometry partial pressure. This delay can be correlated to the fact that the analysis chamber was occupied by O_2 prior to H_2 injection. However, there was a 4.75 min delay between the mass spectrometry detection of the primary 16 Torr H_2 and the H_2O partial pressure increase at time $t \approx 12$ min, suggesting the effective time constant of this non-equilibrium process (including water desorption and time-of-flight) is on the order of 5 min at these partial pressures.

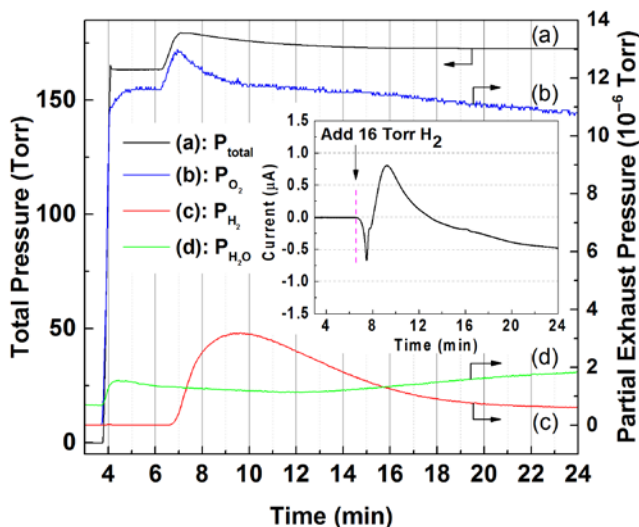


Figure 6. Partial pressure and total pressure kinetics during fast reaction regime. Plot (a) gives total pressure as measured by capacitive pressure transducers, while plots (b) – (d) give partial pressures of exhaust mixture. The inset shows simultaneously measured reaction current.

Moreover, we noticed an interesting behavior that the water concentration begins to increase at time $t \approx 12$ min *concurrently* with the current polarity switch from positive to negative, as seen in Figure 6. This finding provides further proof of a regime change, converting from a thermionic process with positive polarity to a steady-state charge diffusion process with negative polarity resulting in water production. Given that this polarity switch follows the fast reaction region but precedes the slow reaction regime, we advocate this is also further evidence that water

desorption is the rate controlling step of the stationary current mechanism for electrolyte-free samples exhibiting chemical reaction-induced *room temperature* stationary currents.

4. Conclusion

We conclude that Pt/TiO₂/Ti heterojunction nanocomposites, adept at utilizing the catalytic oxidation of hydrogen to convert surface-released chemical energy into a stationary electrical signal, exhibit an upper-limit value of the water turnover frequency with increasing hydrogen concentration. The TOF approaches an asymptotic value, attributed to the saturation of the Pt/TiO₂ interface. It has been proposed that desorption of water is the limiting step of the stationary current generation. The existence of a rate-determining step in the water TOF, in addition to the current polarity reversal simultaneously with the increase in water concentration, provides new evidence toward the production of water as the dominant force behind the generated electromotive force under steady-state room temperature conditions. Furthermore, a time constant for the production of water was determined under the oxyhydrogen pressures investigated. We conclude that reaching a steady state for the entire multi-step process of H₂ adsorption, H₂O formation, and H₂O desorption from the mesoporous Pt/TiO₂ interface at room temperature in 160 Torr O₂ atmosphere requires about 5 min. Results of the present study shed light on the underlying and competing processes within the Pt/TiO₂/Ti system during the oxidation of hydrogen and the generation of a room temperature stationary current. Indeed, optimizing the Pt/TiO₂ interface for increased rate of water desorption may further increase the extraordinary properties of this chemical-electrical transducer.

AUTHOR INFORMATION

Corresponding Author

*E-mail: ekarpov@uic.edu

ACKNOWLEDGMENT

This research was supported by the Center for Nanoscale Materials at Argonne National Laboratory. Use of the Center for Nanoscale Materials, an Office of Science user facility, was supported by the U.S. Department of Energy, Office of Science, Office of Basic Energy Sciences, under Contract No. DE-AC02-06CH11357.

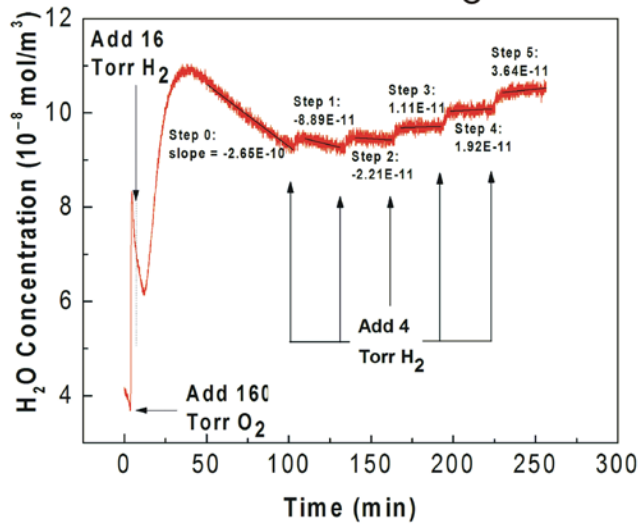
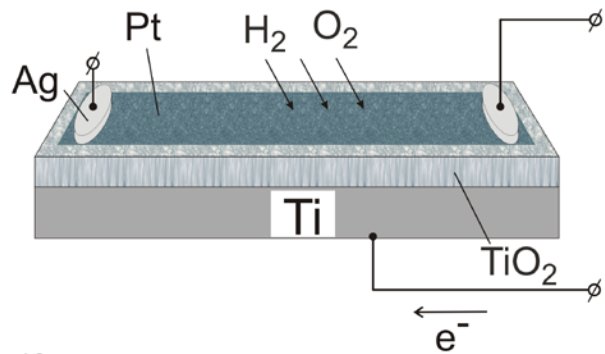
REFERENCES

- (1) Ellis, B. L.; Knauth, K.; Djenizian, T. Three-Dimensional Self-Supported Metal Oxides for Advanced Energy Storage. *Adv. Mater.* **2014**, *26*, 3368–3397.
- (2) Mao, S.; Wen, Z.; Huang, T.; Houa, Y.; Chen, J. High-Performance Bi-Functional Electrocatalysts of 3D Crumpled Graphene–Cobalt Oxide Nanohybrids for Oxygen Reduction and Evolution Reactions. *Energy Environ. Sci.* **2014**, *7*, 609–616.
- (3) Yahiro, H. High Temperature Fuel Cell with Ceria-Yttria Solid Electrolyte. *J. Electrochem. Soc.* **1988**, *135*, 2077.
- (4) Zhou, Y.; Holme, T.; Berry, J.; Ohno, T. R.; Ginley, D.; O’Hayre, R. Dopant-Induced Electronic Structure Modification of HOPG Surfaces: Implications for High Activity Fuel Cell Catalysts. *J. Phys. Chem. C* **2010**, *114*, 506–515.
- (5) Jaouen, F.; Proietti, E.; Lefèvre, M.; Chenitz, R.; Dodelet, J.-P.; Wu, G.; Chung, H. T.; Johnston, C. M.; Zelenay, P. Recent Advances in Non-Precious Metal Catalysis for Oxygen-Reduction Reaction in Polymer Electrolyte Fuel Cells. *Energy Environ. Sci.* **2011**, *4*, 114.

- (6) Zhang, M.; Feng, G.; Song, Z.; Zhou, Y.; Chao, H.; Yuan, D.; Tan, T. T. Y.; Guo, Z.; Hu, Z.; Tang, B. Z.; Liu, B.; Zhou, D. Two-Dimensional Metal–Organic Framework with Wide Channels and Responsive Turn-On Fluorescence for the Chemical Sensing of Volatile Organic Compounds. *J. Am. Chem. Soc.* **2014**, *136*, 7241–7244.
- (7) Hu, Z.; Deibert, B. J.; Li, J. Luminescent Metal–Organic Frameworks for Chemical Sensing and Explosive Detection. *Chem. Soc. Rev.* **2014**, *43*, 5815–5840
- (8) Xu, S.; Zhang, Y.; Jia, L.; Mathewson, K. E.; Jang, K.; Kim, J.; Fu, H.; Huang, X.; Chava, P.; Wang, R.; Bhole, S.; Wang, L.; Na, Y. J.; Guan, Y.; Flavin, M.; Han, Z.; Huang, Y.; Rogers, J. A. Soft Microfluidic Assemblies of Sensors, Circuits, and Radios for the Skin. *Science* **2014**, *344*, 70–74.
- (9) Hübner, T.; Boon-Brett, L.; Black, G.; Banach, U. Hydrogen Sensors - a Review. *Sens. Actuators, B* **2011**, *157*, 329–352.
- (10) Chiu, S. Y.; Tsai, J. H.; Huang, H. W.; Liang, K. C.; Huang, T. H.; Liu, K. P.; Tsai, T. M.; Hsu, K. Y.; Lour, W. S. Hydrogen Sensors with Double Dipole Layers Using a Pd-Mixture-Pd Triple-Layer Sensing Structure. *Sens. Actuators, B* **2009**, *141*, 532–537.
- (11) Nedrygailov, I. I.; Karpov, E. G. Pd/n-SiC Nanofilm Sensor for Molecular Hydrogen Detection in Oxygen Atmosphere. *Sens. Actuators, B* **2010**, *148*, 388–391.
- (12) Thompson, T. L.; Yates, J. T. Surface Science Studies of the Photoactivation of TiO₂-New Photochemical Processes. *Chem. Rev.* **2006**, *106*, 4428–4453.
- (13) Nowotny, M. K.; Sheppard, L. R.; Bak, T.; Nowotny, J. Defect Chemistry of Titanium Dioxide. Application of Defect Engineering in Processing of TiO₂-Based Photocatalysts. *J. Phys. Chem. C* **2008**, *112*, 5275–5300.
- (14) Hagemann, U.; Krix, D.; Nienhaus, H. Electronic Excitations Generated by the Deposition of Mg on Mg Films. *Phys. Rev. Lett.* **2010**, *104*, 028301.

- (15) Hagemann, U.; Nienhaus, H. Quantum Size Effects in Chemicurrent Measurements During Low-Temperature Oxidation of Mg (0001) Epilayers. *New J. Phys.* **2014**, *16*, 113035.
- (16) Diebold, U. The Surface Science of Titanium Dioxide. *Surf. Sci. Rep.* **2003**, *48*, 53–229.
- (17) Karpov, E. G.; Hashemian, M. A.; Dasari, S. K. Chemistry-Driven Signal Transduction in a Mesoporous Pt/TiO₂ System. *J. Phys. Chem. C* **2013**, *117*, 15632–15638.
- (18) Kim, S. M.; Lee, H.; Park, J. Y. Charge Transport in Metal-Oxide Interfaces: Genesis and Detection of Hot Electron Flow and Its Role in Heterogeneous Catalysis. *Catal. Lett.* **2015**, *145*, 299–308.
- (19) Lee, H.; Nedrygailov, I. I.; Lee, C.; Somorjai, G. A.; Park, J. Y. Chemical-Reaction-Induced Hot Electron Flows on Platinum Colloid Nanoparticles under Hydrogen Oxidation: Impact of Nanoparticle Size. *Angew. Chem., Int. Ed.* **2015**, *54*, 2340–2344.
- (20) Schierbaum, K.; El Achhab, M. Generation of an Electromotive Force by Hydrogen-to-Water Oxidation with Pt-Coated Oxidized Titanium Foils. *Phys. Status Solidi A* **2011**, *208*, 2796–2802.
- (21) Hashemian, M. A.; Palacios, E.; Nedrygailov, I. I.; Diesing, D.; Karpov, E. G. Thermal Properties of the Stationary Current in Mesoporous Pt/TiO₂ Structures in an Oxyhydrogen Atmosphere. *ACS Appl. Mater. Interfaces* **2013**, *5*, 12375–12379.
- (22) Ray, N. J.; Hashemian, M. A.; Karpov, E. G. A Stationary Current Effect in Mesoporous Pt/ZrO₂ System under H₂/O₂ Environment. *ACS Appl. Mater. Interfaces* **2015**, *7*, 27749–27754.
- (23) Nienhaus, H. Electronic Excitations by Chemical Reactions on Metal Surfaces. *Surf. Sci. Rep.* **2002**, *45*, 1–78.

- (24) Lee, H.; Nedrygailov, I. I.; Lee, Y. K.; Lee, C.; Choi, H.; Choi, J. S.; Choi, C.; Park, J. Y. Graphene–Semiconductor Catalytic Nanodiodes for Quantitative Detection of Hot Electrons Induced by a Chemical Reaction. *Nano Lett.* **2016**, *16*, 1650–1656.
- (25) Cakabay, O.; Achhab, M. E.; Schierbaum, K. Thermal Properties of Solid-State Pt/TiO₂/Ti Emf Cells Studied by Microcalorimetry. *Appl. Phys. A* **2015**, *118*, 1127–1132.
- (26) Cakabay, O.; Achhab, M. E.; Schierbaum, K. Effect of Water Vapor on Pt/TiO₂/Ti Electromotive Force Cells. *J. Phys. Chem. C* **2016**, *120*, 9061–9067.
- (27) Park, J. Y.; Lee, H.; Renzas, J. R.; Zhang, Y.; Somorjai, G. A. Probing Hot Electron Flow Generated on Pt Nanoparticles with Au/ TiO₂ Schottky Diodes During Catalytic CO Oxidation. *Nano Lett.* **2008**, *8*, 2388–2392.
- (28) Park, J. Y.; Kim, S. M.; Lee, H.; Nedrygailov, I. I. Hot-Electron-Mediated Surface Chemistry: Toward Electronic Control of Catalytic Activity. *Acc. Chem. Res.* **2015**, *48*, 2475–2483.



TOC graphic